J. Chem. Sci. (2020)132:151
https://doi.org/10.1007/s12039-020-01857-3

REGULAR ARTICLE

DFT study of CO_2 catalytic conversion by H_2 over Ni_{13} cluster

QIANG KE[a,*], LIMING KANG[a], XIN CHEN[a,b,c,*] and YOU WU[b]

[a]Center for Computational Chemistry and Molecular Simulation, College of Chemistry and Chemical Engineering, Southwest Petroleum University, Chengdu 610500, China
[b]State Key Laboratory of Oil and Gas Reservoir Geology and Exploitation, Southwest Petroleum University, Chengdu 610500, China
[c]Oil and Gas Field Applied Chemistry Key Laboratory of Sichuan Province, College of Chemistry and Chemical Engineering, Southwest Petroleum University, Chengdu 610500, China
E-mail: qiangke@swpu.edu.cn; chenxin830107@pku.edu.cn

MS received 30 July 2020; revised 15 September 2020; accepted 3 October 2020

Abstract. Understanding the mechanism and selectivity of CO_2 catalytic conversion by H_2 on a specific catalyst is of great significance in the context of renewable energy storage from a societal and technological point of view. In this paper, based on the density functional theory calculations, the possible reaction networks of CO_2 hydrogenation on the Ni_{13} cluster are studied systematically. The adsorption energies of the reaction intermediates at various possible adsorption sites, the reaction energies and the activation energies of each elementary reaction are calculated. The results suggest that the adsorption properties of the CO_2 and the intermediates on the Ni_{13} cluster are different from the specific crystal plane such as Ni(111) surface, and the intermediates are highly activated on the Ni_{13} surface. The most advantageous pathways for the production of HCOOH, CH_3OH, and CH_4 are determined, and the activation barrier of the corresponding rate-determining step is 1.63 eV, 1.55 eV, and 1.55 eV, respectively. This indicates that the Ni_{13} cluster has higher activity towards CO_2 catalytic conversion compared with other catalysts such as Cu(111), Ni(111), and Pt/Ni(111) surface. Furthermore, the H_3CO^* hydrogenation or the dissociation is demonstrated to be the crucial step in determining the selectivity for CH_3OH and CH_4.

Keywords. CO_2 hydrogenation; Ni_{13} cluster; adsorption; reaction mechanism; DFT.

1. Introduction

In recent years, with the depletion of fossil energy and the high cost of other energies, great attention has been paid to the research of new energy.[1] Also, since the industrial revolution burned fossil fuels, the sharp rise in the concentration of carbon dioxide caused a series of problems, such as the global warming, rising sea levels, and ocean acidification.[2–4] The use of CO_2 hydrogenation to synthesize fuels and useful chemicals can not only effectively alleviate the greenhouse effect but also solve the energy problems.[5–8] In particular, using CO_2 hydrogenation to produce formic acid (HCOOH), methanol (CH_3OH), and methane (CH_4) is an effective and feasible solution.[9–18]

However, CO_2 is a kinetically and thermodynamically stable molecule. Generally, the cleavage of the C–O bond requires a high activation barrier, which needs to be reduced by an effective catalyst. An excellent catalyst should have a good activation ability during the hydrogenation process, good ability in C–O bond breakage, and the dissociation of H_2.[19] The transitional metal nickel (Ni) has been used in some hydrogenation reactions such as CO_2 hydrogenation to formic acid, methanol, methane, and so on.[20–27] However, the Ni catalysts in these works are mainly the specific crystal plane or the nanoparticles. And their catalytic properties are different from the small clusters due to different surface atomic arrangement and electronic characteristics. For example, the Ni-based clusters have recently been studied as the ammonia decomposition reaction catalyst,[28] and it indeed shows different catalytic activity from large nanoparticles.[29,30] Therefore, it will be meaningful to investigate the detailed mechanism and the selectivity of the CO_2 hydrogenation reaction on the small Ni cluster. In this paper, the Ni_{13} cluster is selected as the catalytic model due to the following two reasons: (i) Based on the previous researches about the cluster

*For correspondence

Published online: 11 November 2020

size effect,[31–33] the cluster composed by 13 atoms possesses the most suitable size that may lead to properly combine with the CO_2 molecule and available locations for co-adsorption of multiple adsorbents; [33] (ii) Ni_{13} cluster is also demonstrated to have excellent stability among different Ni_n clusters.[34] Therefore, we speculated that the Ni_{13} cluster could effectively catalyze the CO_2 hydrogenation reaction.

In order to explore the CO_2 hydrogenation mechanism and the selectivity of a specific catalyst, screening the possible reaction pathways and identifying the key elementary steps are critical. In this work, the reaction networks for hydrogenation of CO_2 on the Ni_{13} cluster are studied in detail by density functional theory (DFT) method. The adsorption of the reaction intermediates, as well as the activation barrier and the reaction energy of each elementary step involved in the CO_2 hydrogenation, are considered. By comparing the activation barriers of each elementary step, the most favourable pathways for the production of HCOOH, CH_3OH, and CH_4 are obtained. Furthermore, the key elementary steps that control the activity and selectivity of CO_2 hydrogenation on the Ni_{13} cluster are identified.

2. Computational details

All calculations were implemented in Materials Studio with the DMol^3 code.[35,36] The Perdew–Burke–Ernzerhof (PBE) functional of the generalized gradient approximation (GGA) was used to calculate the exchange–correlation energy.[37] The double numerical plus polarization (DNP) and DFT semi-core pseudopotential were chosen during the geometry optimization. The convergence tolerances of energy change, maximum force, and maximum displacement were set as 2×10^{-5} Ha, 0.004 Ha/Å, and 0.005 Å, respectively. All the transition states of the elementary steps were identified by a complete LST/QST approach and a mode-eigenvector following method.[38,39] Frequency calculations were applied to all transition states and the corresponding vibration modes were verified to link reactants and products.

The adsorption energy (E_{ads}) on the Ni_{13} cluster was calculated as $E_{ads} = E_{system} - (E_{intermediate} + E_{catalyst})$, where E_{system}, $E_{intermediate}$, and $E_{catalyst}$ are the total energies of the catalyst with the adsorbed intermediates, the isolated intermediates, and the catalyst, respectively. The reaction energy (ΔE) and the activation barrier (E_a) was calculated as $\Delta E = E_{FS} - E_{IS}$ and $E_a = E_{TS} - E_{IS}$, respectively, where E_{IS}, E_{TS}, and E_{FS} represent the total energies of the initial state (IS), the transition state (TS), and the final state (FS), respectively.

3. Results and Discussions

Based on the experimental and calculation results in previous literature,[19,40–43] we investigated possible reaction networks for the hydrogenation of CO_2 to HCOOH, CH_3OH, and CH_4 on the Ni_{13} cluster, as shown in Figure 1. After the geometry optimization, we found that the Ni_{13} cluster has a stable icosahedral configuration. The optimized structure together with the adsorption sites (including top, bridge, and hollow) are shown in Figure 2.

3.1 *Adsorption configurations and energies of the intermediates on the Ni_{13} cluster*

Based on the reaction networks on the Ni_{13} cluster, we optimized the adsorption structure of all the possible intermediates. The most stable adsorption geometries are shown in Figure 3, and the important bond parameters and adsorption energies are shown in Table 1.

The most stable adsorption sites for H*, C*, and O* are all hollow sites on the Ni_{13} cluster, as shown in Figure 3a-c. The corresponding adsorption energies are − 3.08 eV, − 7.09 eV, and − 6.10 eV, respectively. They are stronger than the corresponding adsorption energies on the Ni(111) surface,[42] which are − 2.81 eV, − 6.78 eV, and − 5.67 eV, respectively. And CO* is adsorbed on the hollow site through the C–Ni bond with an optimized bond length of 1.954 Å. The adsorption energy is − 2.48 eV, which is also stronger than that on the Pt/Ni(111) surface (− 1.83 eV),[19] Ga_3Ni_5(111) surface (− 2.37 eV),[20] and Ni(111) surface (− 1.92 eV).[42] These results indicate that the catalytic property of Ni_{13} cluster is expected different from the specific crystal plane, and all the above intermediates are highly activated on the Ni_{13} cluster.

As shown in Figure 3g, CO_2* is adsorbed at the bridge site. It can be seen that the configuration of the CO_2 molecule no longer maintains the original linear shape. The two C–O bonds are stretched from 1.179 Å (gas phase) to 1.250 Å and 1.264 Å, respectively. And the bond angle is changed to 137.2°. The adsorption energy is − 1.25 eV, which is stronger than that on the Pt/Ni(111) (− 0.15 eV) surface,[19] Ga_3Ni_5(111) surface (− 0.52 eV),[20] and the Mg/Cu(111) surface (− 1.15 eV).[44] Since the CO_2 adsorption is the first

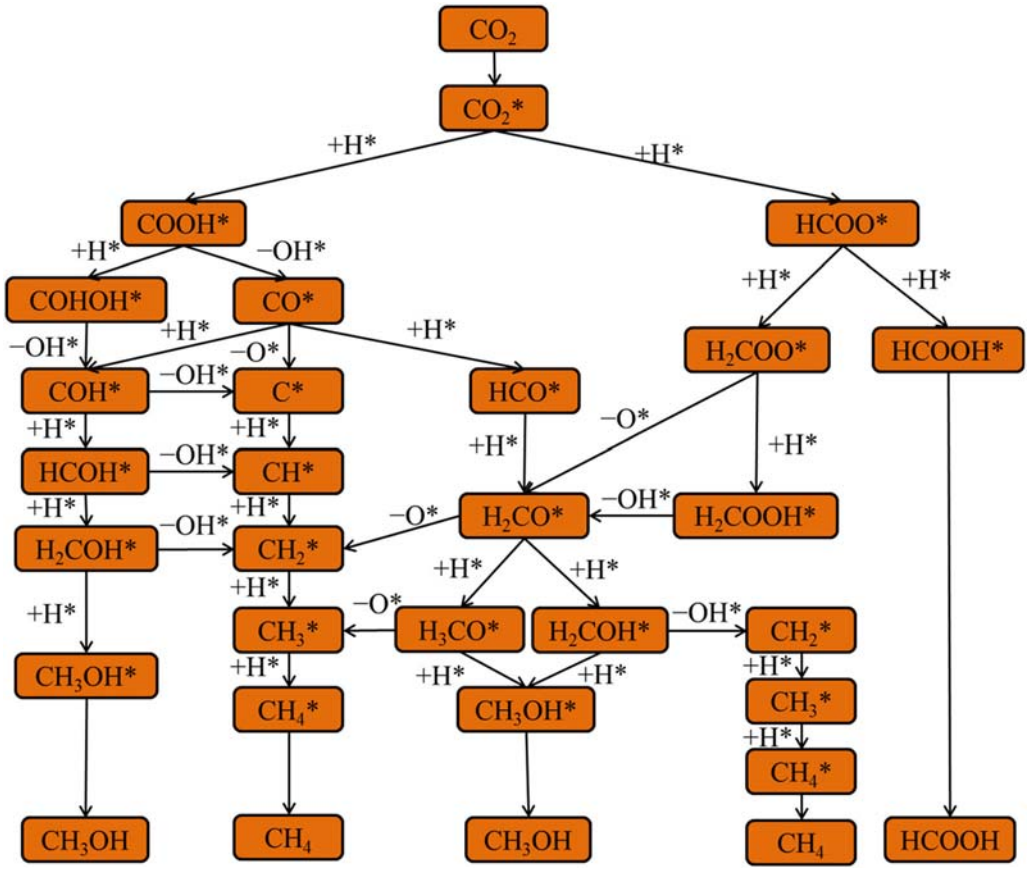

Figure 1. Possible reaction networks of CO_2 hydrogenation on the Ni_{13} cluster.

step of the CO_2 hydrogenation, the highly activated CO_2 molecule may indicate that the Ni_{13} cluster has a higher activity towards CO_2 hydrogenation.

The OH* is adsorbed at the bridge site through the O atom with an adsorption energy of − 3.90 eV. The adsorption site for H_2* is the top site with an adsorption energy of − 0.80 eV. Previous experiments and theoretical studies have shown that HCOO* is an important intermediate for CO_2 hydrogenation.[45–47] Two O atoms of HCOO* are respectively adsorbed on the top site with an adsorption energy of − 4.43 eV.

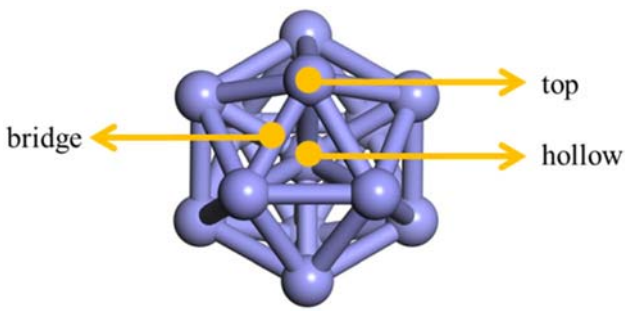

Figure 2. Optimized structure and possible adsorption sites of Ni_{13} cluster.

For H_2COO*, it is widely regarded as the intermediate of CO_2 hydrogenation via HCOO pathway.[32,47,48] The two O of H_2COO* atoms are adsorbed at the bridge site and top site, respectively, and the corresponding bond lengths are 1.968 Å, 1.977 Å, and 1.818 Å, respectively. The adsorption energy is − 4.70 eV, which is stronger than that on the Pt/Ni(111) (− 3.86 eV) surface.[19] The COOH* is adsorbed at the bridge site with an adsorption energy of − 3.41 eV. For HCOOH* and COHOH*, the top site is the most favourable adsorption site and their adsorption energies are − 1.23 eV and − 2.80 eV, respectively. For H_2COOH*, two O atoms are adsorbed at the bridge site and the top site respectively, and the adsorption energy is − 3.52 eV.

Figure 3m-p show the adsorption of CH_x (x = 1–4) species. The adsorption site for CH* is the hollow site with an adsorption energy of − 6.69 eV, which is close to the value of − 6.64 eV[19] and − 6.63 eV[49] over the Pt/Ni(111) surface. The adsorption sites for CH_2* and CH_3* are all bridge site and their adsorption energies are − 4.63 eV and − 2.64 eV, respectively. The adsorption site for CH_4* is the top site with an adsorption energy of − 0.42 eV.

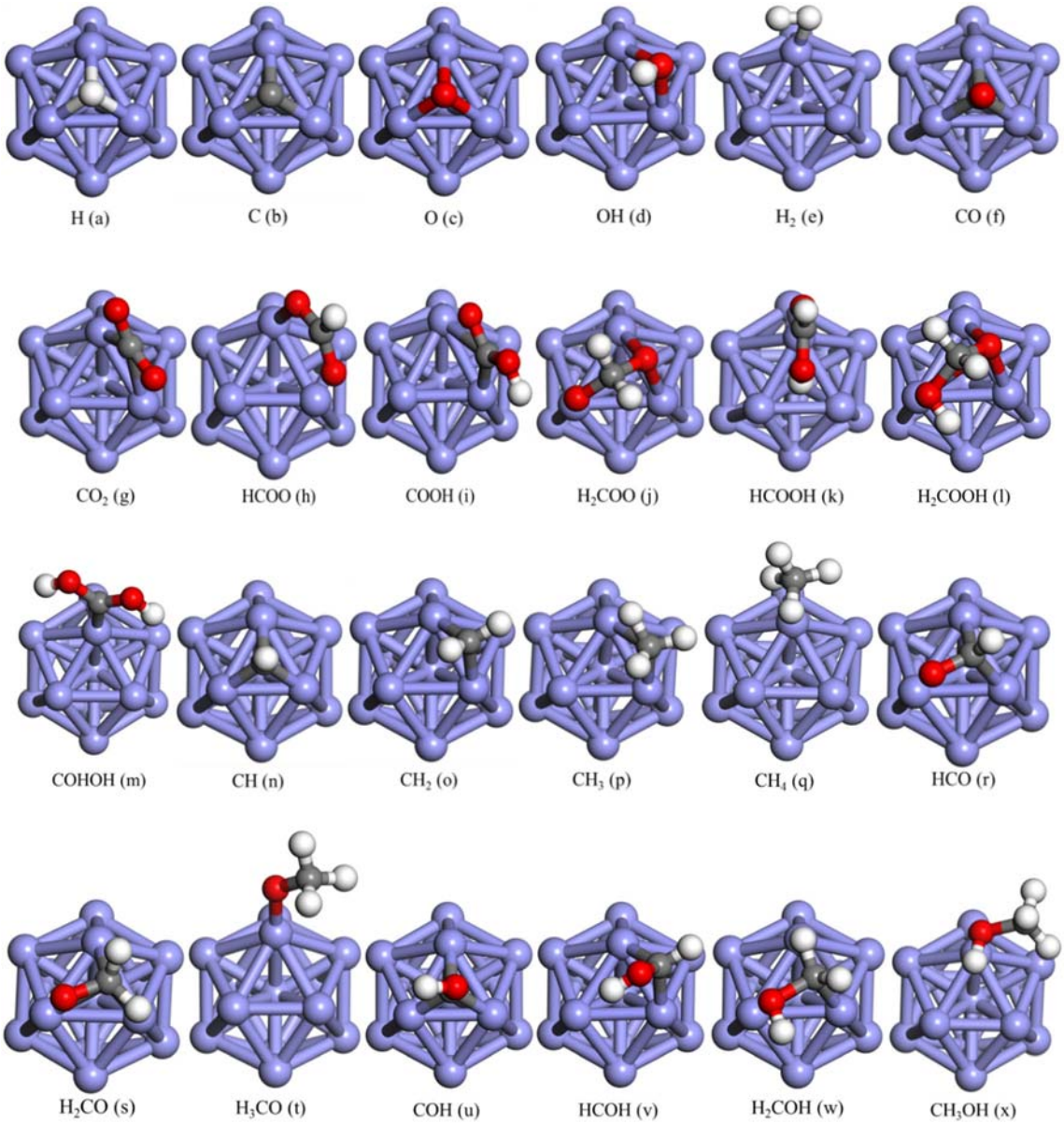

Figure 3. Stable adsorption configurations of all possible intermediates in the hydrogenation of CO_2 on the Ni_{13} cluster. The blue, gray, white, and red balls represent Ni, C, H, and O atom, respectively.

For H_xCO (x = 1–3) species (Figure 3q-s), it can be observed that both HCO* and H_2CO* are interacted with the Ni_{13} cluster through their C and O atoms. The interaction mode of HCO* is the same as it is on the Mg/Cu(111) catalyst studied by Santiago-Rodríguez et al. [44] Furthermore, the H_3CO* is adsorbed at the top site of Ni_{13} cluster via O atom and the bond length of O–Ni is 1.787 Å.

For H_xCOH (x = 0–3) species (Figure 3t-w), the most stable adsorption site for COH* is the hollow site with an adsorption energy of − 4.80 eV, which is the same as the value over the Pt/Ni(111) surface.[19] The HCOH* and H_2COH* are stably adsorbed at the bridge site via their C atoms with the adsorption energy of − 3.65 eV and − 2.56 eV, respectively. The most stable adsorption site of CH_3OH* is the top site with an adsorption energy of − 0.81 eV.

3.2 *Reaction pathways on the Ni_{13} cluster*

After determining the most stable adsorption structure, the feasible reaction pathways for the hydrogenation of CO_2 to HCOOH, CH_3OH, and CH_4 on the Ni_{13} cluster are therefore be calculated. The transition state of each elementary step has been searched and determined. The activation barrier (E_a) and the reaction energy (ΔE) have been obtained, as clearly shown in

Table 1. The most stable adsorption site, bond parameters, and the adsorption energies (E_{ads}) in CO_2 hydrogenation on the Ni_{13} cluster.

Species	Site	Bond parameters (Å)	E_{ads} (eV)
H	hollow	d_{H-Ni} = 1.767, 1.767, 1.777	− 3.08
C	hollow	d_{C-Ni} = 1.778, 1.779, 1.779	− 7.09
O	hollow	d_{O-Ni} = 1.882, 1.892, 1.892	− 6.10
OH	bridge	d_{O-Ni} = 1.970, 1.970	− 3.90
H_2	top	d_{H-Ni} = 1.571	− 0.80
CO	hollow	d_{C-Ni} = 1.954, 1.954, 1.954	− 2.48
CO_2	bridge	d_{C-Ni} = 1.856, 2.287	− 1.25
HCOO	top-top	d_{O-Ni} = 1.935, 1.935	− 4.43
COOH	bridge	d_{C-Ni} = 1.861, 2.523	− 3.41
H_2COO	bridge-top	d_{O-Ni} = 1.968, 1.977, 1.818	− 4.70
HCOOH	top	d_{O-Ni} = 1.946	− 1.23
H_2COOH	bridge-top	d_{O-Ni} = 2.018, 2.039, 2.097	− 3.52
COHOH	top	d_{C-Ni} = 1.794	− 2.80
CH	hollow	d_{C-Ni} = 1.867, 1.869, 1.870	− 6.69
CH_2	bridge	d_{C-Ni} = 1.907, 1.910	− 4.63
CH_3	bridge	d_{C-Ni} = 2.024, 2.107	− 2.64
CH_4	top	d_{C-Ni} = 2.449	− 0.42
HCO	bridge-top	d_{C-Ni} = 1.939, 1.951, d_{O-Ni} = 1.923	− 3.26
H_2CO	bridge-top	d_{C-Ni} = 2.047, 2.065, d_{O-Ni} = 1.873	− 1.83
H_3CO	top	d_{O-Ni} = 1.787	− 2.97
COH	hollow	d_{C-Ni} = 1.871, 1.879, 1.896	− 4.80
HCOH	bridge	d_{C-Ni} = 1.926, 1.931	− 3.65
H_2COH	bridge-top	d_{C-Ni} = 1.991, 2.105, d_{O-Ni} = 2.102	− 2.56
CH_3OH	top	d_{O-Ni} = 2.082	− 0.81

Table 2. The initial state (IS), transition state (TS), and the final state (FS) of each elementary step in Table 2 are shown in Figure 4.

H_2 dissociation. The dissociation of H_2* into H* (R1) atoms is a key step in the hydrogenation of CO_2. As shown in Figure 4, the H_2* is adsorbed at the top site of one Ni atom at the initial state and then be cleaved. This reaction is exothermic ($\Delta E = -0.72$ eV) with a small activation barrier of 0.21 eV, indicating it is thermodynamically and kinetically favourable.

CO_2 hydrogenation. After the CO_2* and the H* are co-adsorbed on the Ni_{13} cluster, the following reaction between them involves two competitive pathways: one is the adsorbed H* attacks the C atom of CO_2* to form HCOO* (R2), and the other is the H* combines the O atom to form COOH* (R3). The E_a of R2 is 0.88 eV and the ΔE is − 0.39 eV, which is 0.99 eV and 0.96 eV lower than the corresponding value of R3. Therefore, the formation of HCOO* is both thermodynamically and kinetically favourable.

HCOO hydrogenation. The product of HCOO* hydrogenation is HCOOH* or H_2COO*. When the H* is combined with the O atom of HCOO* (R4), the HCOOH* is formed. The calculated activation barrier is 1.63 eV and the reaction energy is 1.56 eV. On the contrary, the H_2COO* is formed when the C atom of HCOO* is attacked by the H* to generate a C–H bond (R5). This reaction is endothermic (1.02 eV) with an activation barrier of 1.55 eV. Therefore, HCOO* hydrogenation to form the H_2COO* is thermodynamically and kinetically more favourable. For H_2COO, there are two competitive pathways for the further reaction of H_2COO*. One is the direct decomposition of H_2COO* to generate the H_2CO* and O* (R6), the other is the further hydrogenation to form the H_2COOH* (R7). The R6 needs to overcome a small activation barrier (0.63 eV) when compared with R7 (1.37 eV), indicating the H_2COO* is prone to be decomposed.

COOH dissociation or hydrogenation. The COOH* can be decomposed into CO* and OH* (R9). It is an exothermic reaction (− 1.24 eV) with an activation barrier of 0.99 eV. Also, COOH* can also be hydrogenated to form COHOH* (R10). The reaction has a higher activation barrier of 1.73 eV, with reaction energy of 1.09 eV. The dissociation of COOH* is more likely to occur on the Ni_{13} cluster.

CO dissociation or hydrogenation. The direct dissociation of CO* is slightly endothermic (R12, ΔE = 0.39 eV). This step has a higher activation

Table 2. Activation barriers (E_a, eV) and reaction energies (ΔE, eV) of each elementary step.

	Step	E_a	ΔE
R1	$H_2 + 2^* \rightarrow H^* + H^*$	0.21	− 0.72
R2	$CO_2^* + H^* \rightarrow HCOO^* + *$	0.88	− 0.39
R3	$CO_2^* + H^* \rightarrow COOH^* + *$	1.87	0.57
R4	$HCOO^* + H^* \rightarrow HCOOH^* + *$	1.63	1.56
R5	$HCOO^* + H^* \rightarrow H_2COO^* + *$	1.55	1.02
R6	$H_2COO^* + * \rightarrow H_2CO^* + O^*$	0.63	− 0.36
R7	$H_2COO^* + H^* \rightarrow H_2COOH^* + *$	1.37	0.83
R8	$H_2COOH^* \rightarrow H_2CO^* + OH^*$	0.69	− 0.64
R9	$COOH^* + * \rightarrow CO^* + OH^*$	0.99	− 1.24
R10	$COOH^* + H^* \rightarrow COHOH^* + *$	1.73	1.09
R11	$COHOH^* + * \rightarrow COH^* + OH^*$	0.91	− 0.96
R12	$CO^* + * \rightarrow C^* + O^*$	2.92	0.39
R13	$CO^* + H^* \rightarrow HCO^* + *$	1.45	1.05
R14	$CO^* + H^* \rightarrow COH^* + *$	2.53	1.50
R15	$HCO^* + H^* \rightarrow H_2CO^* + *$	0.66	0.39
R16	$H_2CO^* + * \rightarrow CH_2^* + O^*$	1.45	− 0.75
R17	$H_2CO^* + H^* \rightarrow H_3CO^* + *$	0.85	0.22
R18	$H_2CO^* + H^* \rightarrow H_2COH^* + *$	1.26	0.52
R19	$H_3CO^* + * \rightarrow CH_3^* + O^*$	0.85	− 1.15
R20	$H_3CO^* + H^* \rightarrow CH_3OH^* + *$	0.79	0.73
R21	$COH^* + * \rightarrow C^* + OH^*$	0.96	− 0.57
R22	$COH^* + H^* \rightarrow HCOH^* + *$	0.74	0.44
R23	$HCOH^* + * \rightarrow CH^* + OH^*$	0.52	− 1.12
R24	$HCOH^* + H^* \rightarrow H_2COH^* + *$	0.83	0.27
R25	$H_2COH^* + * \rightarrow CH_2^* + OH^*$	0.23	− 1.40
R26	$H_2COH^* + H^* \rightarrow CH_3OH^* + *$	0.92	0.30
R27	$C^* + H^* \rightarrow CH^* + *$	0.65	− 0.38
R28	$CH^* + H^* \rightarrow CH_2^* + *$	0.67	0.57
R29	$CH_2^* + H^* \rightarrow CH_3 + *$	0.66	0.01
R30	$CH_3^* + H^* \rightarrow CH_4^* + *$	0.86	0.29

barrier (2.92 eV), which is higher than that on the Ni(111) surface (2.46 eV) [22] and the Ce–Ni(111) surface (1.66 eV).[50] Therefore, the Ni_{13} cluster has an excellent ability to suppress carbon deposition compared with pure Ni and Ni alloys. For CO* hydrogenation, the hydrogenation product is HCO* or COH*, which depends on whether H* attacks the C or O atom of CO* (R13 or R14). The activation barrier of the R14 (2.53 eV) is significantly higher than that of the R13 (1.45 eV). Therefore, from the kinetics point of view, HCO* formation is easy to occur on the Ni_{13} cluster.

HCO hydrogenation. HCO* can be hydrogenated to form H_2CO^* (R15). This reaction needs to overcome a small activation barrier (0.66 eV) and it is endothermic (0.39 eV). The generated H_2CO^* is more likely to be further hydrogenated rather than to be decomposed (R16, E_a = 1.45 eV). The hydrogenation of H_2CO^* involves two competitive pathways: one is the adsorbed H* attacks the C atom of H_2CO^* to form H_3CO^* (R17), and the other is the H* combines the O atom to form H_2COH^* (R18). The activation barrier of R17 is 0.85 eV, which is 0.41 eV lower than that of R18. Hence, the formation of H_3CO^* is more favourable in the competitive reaction based on the reaction kinetics. The activation barrier of H_3CO^* dissociate to CH_3^*+ O* (R19) is calculated to be 0.85 eV, which is similar to that of $H_3CO^* \rightarrow CH_3OH^*$ (R20, E_a = 0.79 eV). The further hydrogenation of CH_3^* to CH_4^* also has a similar activation barrier of 0.86 eV. Therefore, these competitive pathways determine whether the product is CH_4 or CH_3OH.

COH dissociation or hydrogenation. COH* can be decomposed into C* and OH* (R21). Although the reaction is exothermic (− 0.57 eV), it needs to overcome an activation barrier of 0.96 eV. Also, COH* can also be hydrogenated to form HCOH* (R22), with a lower activation barrier of 0.74 eV. It is clear that the R22 is more likely to occur from the kinetics. And HCOH* can be decomposed into CH* and OH* (R23). The process is exothermic (− 1.12 eV) with a lower activation barrier of 0.52 eV. The HCOH* can also be hydrogenated to form H_2COH^* (R24), which has an activation barrier of 0.83 eV with reaction energy of 0.27 eV. It can be seen from both kinetics and thermodynamics that HCOH* is more easily dissociated. For H_2COH^* dissociation (R25), this step needs to overcome a small activation barrier (0.23 eV) and it is exothermic (− 1.40 eV), indicating that the reaction is prone to occur.

CH_x (x = 0–3) hydrogenation. The activation barrier is 0.65 eV for $C^* \rightarrow CH^*$ (R27), 0.67 eV for $CH^* \rightarrow CH_2^*$ (R28), 0.66 eV for $CH_2^* \rightarrow CH_3^*$ (R29), and 0.86 eV for $CH_3^* \rightarrow CH_4^*$ (R30), respectively. The corresponding reaction energies are − 0.38 eV, 0.57 eV, 0.01 eV, and 0.29 eV, respectively. The calculation results show that all the steps of CH_x hydrogenation are feasible.

3.3 *General discussions*

The possible reaction networks of CO_2 hydrogenation on the Ni_{13} cluster have been studied, and the activation barriers and reaction energies of all the elementary steps have been obtained and compared. The optimized pathways for the production of HCOOH, CH_3OH, and CH_4 are determined. The HCOOH is mainly produced by the steps of $CO_2^* \rightarrow HCOO^* \rightarrow HCOOH^*$. The rate-determining step is recognized as $HCOO^* \rightarrow HCOOH^*$, with an activation barrier of 1.63 eV. The CH_3OH is determined to be formed by the reactions of $CO_2^* \rightarrow HCOO^* \rightarrow H_2COO^* \rightarrow H_2CO^* \rightarrow H_3CO^* \rightarrow CH_3OH^*$. The rate-determining step is $HCOO^* \rightarrow H_2COO^*$, which has an activation barrier of 1.55 eV. The rate-determining step of the production of CH_4 is also this step,

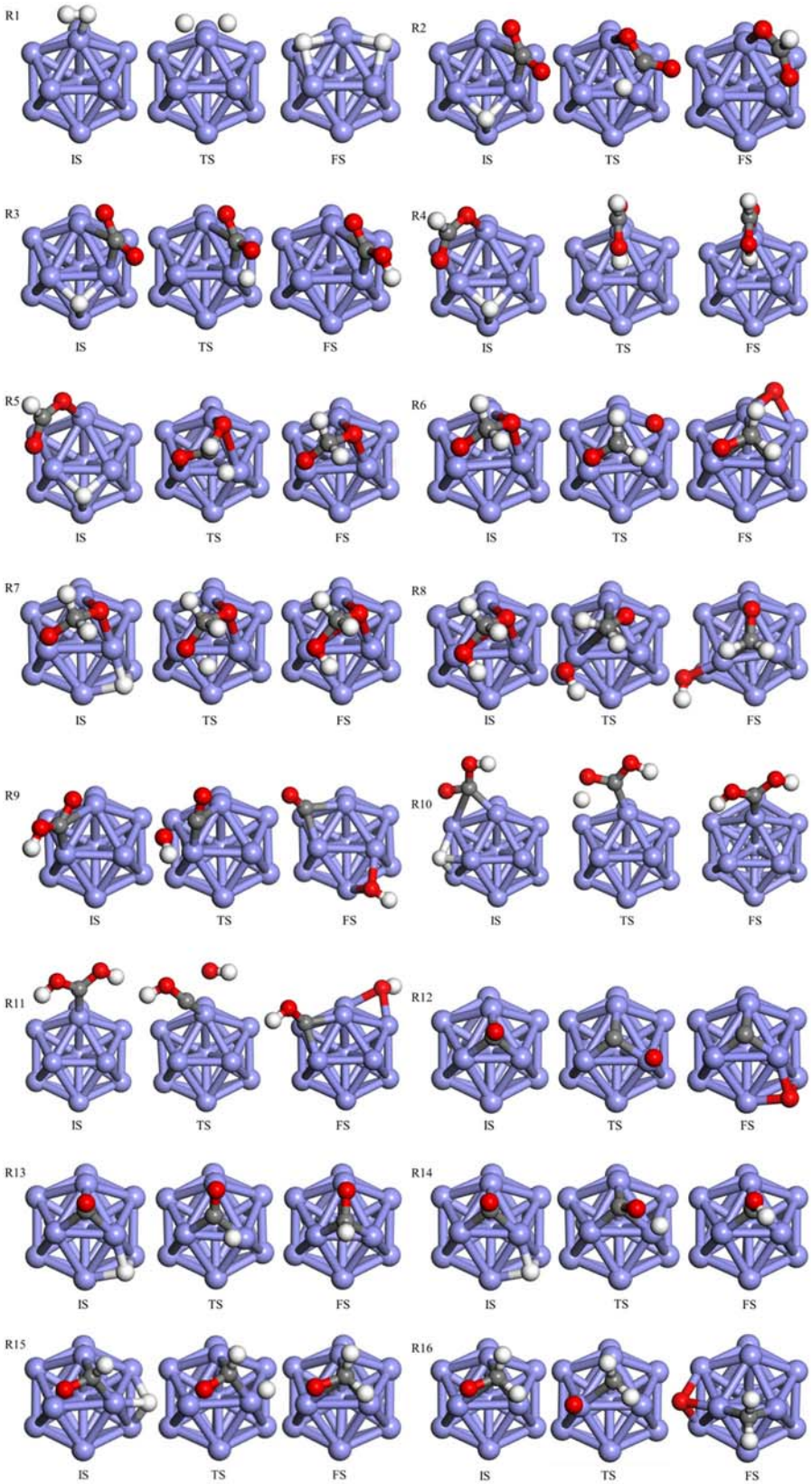

Figure 4. The initial state (IS), transition state (TS), and the final state (FS) of each elementary step.

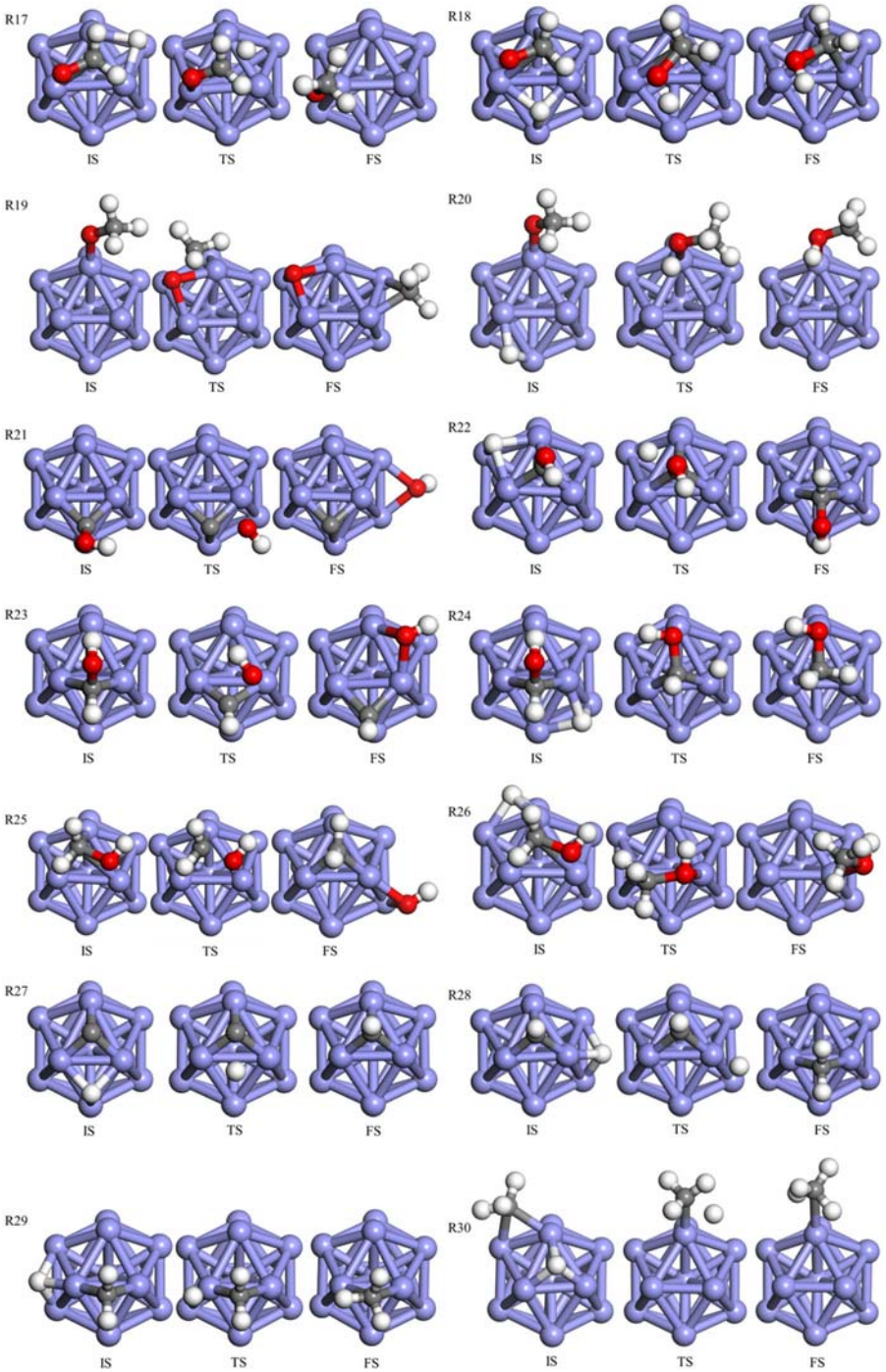

Figure 4. continued

as clearly shown in Figure 5. Notably, the hydrogenation of H_3CO^* and its dissociation into CH_3^* are competitive, which determines the selectivity for CH_3OH and CH_4. Also, the 1.55 eV activation barrier of the rate-determining step on the Ni_{13} cluster is lower than that on many other catalysts such as the Cu(111) surface (1.60 eV),[18] Pt/Ni(111) surface (2.07 eV),[19] the Ni(111) (2.46 eV) surface,[22] and the Cu_{13} cluster (1.60 eV).[51]

4. Conclusions

In this work, the possible reaction networks for CO_2 hydrogenation on the Ni_{13} cluster are studied in detail based on the DFT method. The most stable adsorption structures of all the possible intermediates, as well as the activation barriers and reaction energies of each elementary reaction, are calculated. The results uncover that the adsorption properties of the intermediates are different

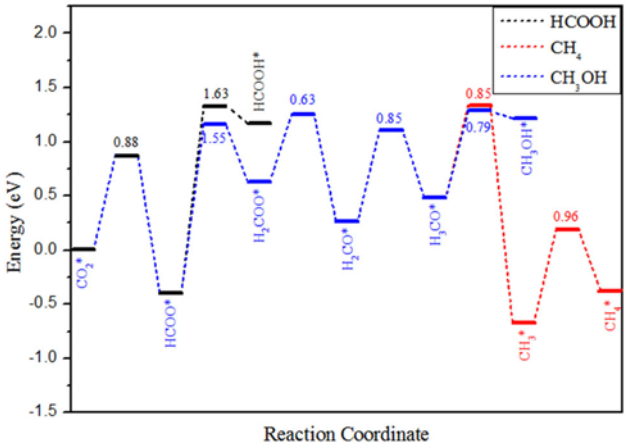

Figure 5. The optimized pathways for the production of HCOOH, CH_3OH, and CH_4 on the Ni_{13} cluster.

from the specific crystal plane such as Ni(111) surface, and the intermediates are highly activated on the Ni_{13} cluster based on the calculated adsorption energies. In particular, the CO_2 no longer maintains the original linear structure and is strongly adsorbed on the surface through chemical adsorption. By comparing the activation barriers of each elementary step, the optimized pathways for the production of HCOOH, CH_3OH, and CH_4 are determined, which are $CO_2^* \rightarrow HCOO^* \rightarrow HCOOH^*$, $CO_2^* \rightarrow HCOO^* \rightarrow H_2COO^* \rightarrow H_2CO^* \rightarrow H_3CO^* \rightarrow CH_3OH^*$, and $CO_2^* \rightarrow HCOO^* \rightarrow H_2COO^* \rightarrow H_2CO^* \rightarrow H_3CO^* \rightarrow CH_3^* \rightarrow CH_4^*$, respectively. The 1.55 eV activation barrier of the rate-determining step for the production of CH_3OH or CH_4 is lower than that on many other catalysts such as the Pt/Ni(111) and the Ni(111) surface. Moreover, we demonstrate that the H_3CO^* hydrogenation or the dissociation determines the selectivity for CH_3OH and CH_4, which provides a guideline for designing high selective catalyst for CO_2 hydrogenation. In general, based on the calculated activation barriers, it can be found that the Ni_{13} cluster not only has excellent ability to suppress carbon deposition but also has high CO_2 hydrogenation activity.

Acknowledgements

This work is supported by the Applied Basic Research Project of Science and Technology Department of Sichuan Province (2020YJ0418), the Youth Science and Technology Innovation Team of Southwest Petroleum University (2018CXTD05), and the Open Fund of State Key Laboratory of Oil and Gas Reservoir Geology and Exploitation of Southwest Petroleum University (PLN201925). We acknowledge the National Supercomputing Center in Shenzhen for providing the computational resources and Materials Studio software.

References

1. Wu G, Zeng M, Peng L, Liu X, Li B and Duan J 2016 China's new energy development: Status, constraints and reforms *Renew. Sustain. Energy Rev.* **53** 885
2. Wang L, Chen W, Zhang D, Du Y, Amal R, Qiao S, Wu J and Yin Z 2019 Surface strategies for catalytic CO_2 reduction: From two-dimensional materials to nanoclusters to single atoms *Chem. Soc. Rev.* **48** 5310
3. Caldeira K and Wickett M E 2003 Anthropogenic carbon and ocean pH *Nature* **425** 365
4. Masson-Delmotte V, Kageyama M, Braconnot P, Charbit S, Krinner G, Ritz C, Guilyardi E, Jouzel J, Abe-Ouchi A, Crucifix M, Gladstone R M, Hewitt C D, Kitoh A, LeGrande A N, Marti O, Merkel U, Motoi T, Ohgaito R, Otto-Bliesner B, Peltier W R, Ross I, Valdes P J, Vettoretti G, Weber S L, Wolk F and Yu Y 2006 Past and future polar amplification of climate change: Climate model intercomparisons and ice-core constraints *Clim. Dyn.* **26** 513
5. Aresta M and Dibenedetto A 2007 Utilisation of CO_2 as a chemical feedstock: Opportunities and challenges *Dalton Trans.* **28** 2975
6. Appel A M, Bercaw J E, Bocarsly A B, Dobbek H, DuBois D L, Dupuis M, Ferry J G, Fujita E, Hille R, Kenis P J A, Kerfeld C A, Morris R H, Peden C H F, Portis A R, Ragsdale S W, Rauchfuss T B, Reek J N H, Seefeldt L C, Thauer R K and Waldrop G L 2013 Frontiers, opportunities, and challenges in biochemical and chemical catalysis of CO_2 fixation *Chem. Rev.* **113** 6621
7. Aresta M, Dibenedetto A and Angelini A 2014 Catalysis for the valorization of exhaust carbon: From CO_2 to chemicals, materials, and fuels. Technological use of CO_2 *Chem. Rev.* **114** 1709
8. Wang W-H, Himeda Y, Muckerman J T, Manbeck G F and Fujita E 2015 CO_2 hydrogenation to formate and methanol as an alternative to photo- and electrochemical CO_2 reduction *Chem. Rev.* **115** 12936
9. Boretti A 2013 Renewable hydrogen to recycle CO_2 to methanol *Int. J. Hydrog. Energy* **38** 1806
10. Atsonios K, Panopoulos K D and Kakaras E 2016 Thermocatalytic CO_2 hydrogenation for methanol and ethanol production: Process improvements *Int. J. Hydrog. Energy* **41** 792
11. Tada S, Ikeda S, Shimoda N, Honma T, Takahashi M, Nariyuki A and Satokawa S 2017 Sponge Ni catalyst with high activity in CO_2 methanation *Int. J. Hydrog. Energy* **42** 30126
12. Zhou R, Rui N, Fan Z and Liu C-J 2016 Effect of the structure of Ni/TiO_2 catalyst on CO_2 methanation *Int. J. Hydrog. Energy* **41** 22017
13. Li Y, Chan S H and Sun Q 2015 Heterogeneous catalytic conversion of CO_2: A comprehensive theoretical review *Nanoscale* **7** 8663
14. Yang B, Liu C, Halder A, Tyo E C, Martinson A B F, Seifert S, Zapol P, Curtiss L A and Vajda S 2017 Copper cluster size effect in methanol synthesis from CO_2 *J. Phys. Chem. C* **121** 10406
15. Ye J, Liu C, Mei D and Ge Q 2013 Active oxygen vacancy site for methanol synthesis from CO_2 hydrogenation on In_2O_3(110): A DFT study *ACS Catal.* **3** 1296

16. Iablokov V, Beaumont S K, Alayoglu S, Pushkarev V V, Specht C, Gao J, Alivisatos A P, Kruse N and Somorjai G A 2012 Size-controlled model Co nanoparticle catalysts for CO_2 hydrogenation: Synthesis, characterization, and catalytic reactions *Nano Lett.* **12** 3091
17. Miao B, Ma S S K, Wang X, Su H and Chan S H 2016 Catalysis mechanisms of CO_2 and CO methanation *Catal. Sci. Technol.* **6** 4048
18. Yang Y, Evans J, Rodriguez J A, White M G and Liu P 2010 Fundamental studies of methanol synthesis from CO_2 hydrogenation on Cu(111), Cu clusters, and Cu/ZnO(0001) *Phys. Chem. Chem. Phys.* **12** 9909
19. Ou Z, Qin C, Niu J, Zhang L and Ran J 2019 A comprehensive DFT study of CO_2 catalytic conversion by H_2 over Pt-doped Ni catalysts *Int. J. Hydrog. Energy* **44** 819
20. Tang Q, Shen Z, Russell C K and Fan M 2018 Thermodynamic and kinetic study on carbon dioxide hydrogenation to methanol over a $Ga_3Ni_5(111)$ surface: The effects of step edge *J. Phys. Chem. C* **122** 315
21. Nizio M, Albarazi A, Cavadias S, Amouroux J, Galvez M E and Da Costa P 2016 Hybrid plasma-catalytic methanation of CO_2 at low temperature over ceria zirconia supported Ni catalysts *Int. J. Hydrog. Energy* **41** 11584
22. Ren J, Guo H, Yang J, Qin Z, Lin J and Li Z 2015 Insights into the mechanisms of CO_2 methanation on Ni(111) surfaces by density functional theory *Appl. Surf. Sci.* **351** 504
23. Peng G, Sibener S J, Schatz G C and Mavrikakis M 2012 CO_2 hydrogenation to formic acid on Ni(110) *Surf. Sci.* **606** 1050
24. Peng G, Sibener S J, Schatz G C, Ceyer S T and Mavrikakis M 2012 CO_2 hydrogenation to formic acid on Ni(111) *J. Phys. Chem. C* **116** 3001
25. Rodriguez J A, Evans J, Feria L, Vidal A B, Liu P, Nakamura K and Illas F 2013 CO_2 hydrogenation on Au/TiC, Cu/TiC, and Ni/TiC catalysts: Production of CO, methanol, and methane *J. Catal.* **307** 162
26. Ye R-P, Li Q, Gong W, Wang T, Razink J J, Lin L, Qin Y-Y, Zhou Z, Adidharma H, Tang J, Russell A G, Fan M and Yao Y-G 2020 High-performance of nanostructured Ni/CeO_2 catalyst on CO_2 methanation *Appl. Catal. B: Environ.* **268** 118474
27. Liu M-H, Chen H-A, Chen C-S, Wu J-H, Wu H-C and Yang C-M 2019 Tiny Ni particles dispersed in platelet SBA-15 materials induce high efficiency for CO_2 methanation *Nanoscale* **11** 20741
28. Chen S, Chen X and Zhang H 2017 Probing the activity of Ni_{13}, Cu_{13}, and $Ni_{12}Cu$ clusters towards the ammonia decomposition reaction by density functional theory *J. Mater. Sci.* **52** 3162
29. Chen S, Chen X and Zhang H 2017 Nanoscale size effect of octahedral nickel catalyst towards ammonia decomposition reaction *Int. J. Hydrog. Energy* **42** 17122
30. 30.Chen X, Zhou J, Chen S and Zhang H 2018 Catalytic performance of M@Ni (M = Fe, Ru, Ir) core–shell nanoparticles towards ammonia decomposition for CO_x-free hydrogen production *J. Nanopart. Res.* **20** 148
31. Ye J, Liu C-j, Mei D and Ge Q 2014 Methanol synthesis from CO_2 hydrogenation over a Pd_4/In_2O_3 model catalyst: A combined DFT and kinetic study *J. Catal.* **317** 44
32. Gu X-K and Li W-X 2010 First-principles study on the origin of the different selectivities for methanol steam reforming on Cu(111) and Pd(111) *J. Phys. Chem. C* **114** 21539
33. Saputro A G, Putra R I D, Maulana A L, Karami M U, Pradana M R, Agusta M K, Dipojono H K and Kasai H 2019 Theoretical study of CO_2 hydrogenation to methanol on isolated small Pd_x clusters *J. Energy Chem.* **35** 79
34. Grigoryan V G and Springborg M 2001 A theoretical study of the structure of Ni clusters (Ni_N) *Phys. Chem. Chem. Phys.* **3** 5135
35. Delley B 2000 From molecules to solids with the $DMol^3$ approach *J. Chem. Phys.* **113** 7756
36. Delley B 1990 An all-electron numerical method for solving the local density functional for polyatomic molecules *J. Chem. Phys.* **92** 508
37. Perdew J P, Burke K and Ernzerhof M 1996 Generalized gradient approximation made simple *Phys. Rev. Lett.* **77** 3865
38. Halgren T A and Lipscomb W N 1997 The synchronous-transit method for determining reaction pathways and locating molecular transition states *Chem. Phys. Lett.* **49** 225
39. Govind N, Petersen M, Fitzgerald G, King-Smith D and Andzelm J 2003 A generalized synchronous transit method for transition state location *Comput. Mater. Sci.* **28** 250
40. Nerlov J, Sckerl S, Wambach J and Chorkendorff I 2000 Methanol synthesis from CO_2, CO and H_2 over Cu(100) and Cu(100) modified by Ni and Co *Appl. Catal. A: Gen.* **191** 97
41. Zhou M and Liu B 2015 DFT investigation on the competition of the water–gas shift reaction versus methanation on clean and potassium-modified nickel(111) surfaces *ChemCatChem* **7** 3928
42. Zhu Y-A, Chen D, Zhou X-G and Yuan W-K 2009 DFT studies of dry reforming of methane on Ni catalyst *Catal. Today* **148** 260
43. Wang Y, Su Y, Zhu M and Kang L 2015 Mechanism of CO methanation on the Ni_4/γ-Al_2O_3 and Ni_3Fe/γ-Al_2O_3 catalysts: A density functional theory study *Int. J. Hydrog. Energy* **40** 8864
44. Santiago-Rodríguez Y, Barreto-Rodríguez E and Curet-Arana M C 2016 Quantum mechanical study of CO_2 and CO hydrogenation on Cu(111) surfaces doped with Ga, Mg, and Ti *J. Mol. Catal. A: Chem.* **423** 319
45. Zhang R, Wang B, Liu H and Ling L 2011 Effect of surface hydroxyls on CO_2 hydrogenation over Cu/γ-Al_2O_3 catalyst: A theoretical study *J. Phys. Chem. C* **115** 19811
46. Rasmussen P B, Holmblad P M, Askgaard T, Ovesen C V, Stoltze P, Nørskov J K and Chorkendorff I 1994 Methanol synthesis on Cu(100) from a binary gas mixture of CO_2 and H_2 *Catal. Lett.* **26** 373
47. Liu L, Yao H, Jiang Z and Fang T 2018 Theoretical study of methanol synthesis from CO_2 hydrogenation on $PdCu_3(111)$ surface *Appl. Surf. Sci.* **451** 333
48. Askgaard T S, Nørskov J K, Ovesen C V and Stoltze P 1995 A kinetic model of methanol synthesis *J. Catal.* **156** 229

49. Zhang M, Yang K, Zhang X and Yu Y 2014 Effect of Ni(111) surface alloying by Pt on partial oxidation of methane to syngas: A DFT study *Surf. Sci.* **630** 236
50. Li K, Yin C, Zheng Y, He F, Wang Y, Jiao M, Tang H and Wu Z 2016 DFT study on the methane synthesis from syngas on a cerium-doped Ni(111) surface *J. Phys. Chem. C* **120** 23030
51. Zhang X, Liu J-X, Zijlstra B, Filot I A W, Zhou Z, Sun S and Hensen E J M 2018 Optimum Cu nanoparticle catalysts for CO_2 hydrogenation towards methanol *Nano Energy* **43** 200